Journal of Power Sources 267 (2014) 527–532

Contents lists available at ScienceDirect

Journal of Power Sources

journal homepage: www.elsevier.com/locate/jpowsour

Novel palladium flower-like nanostructured networks for electrocatalytic oxidation of formic acid

Mingjun Ren [a, b], Liangliang Zou [a, b], Ting Yuan [a, *], Qinghong Huang [a], Zhiqing Zou [a], Xuemei Li [a], Hui Yang [a, *]

[a] Shanghai Advanced Research Institute, Chinese Academy of Sciences, Shanghai 201210, China
[b] University of Chinese Academy of Sciences, Beijing 100039, China

HIGHLIGHTS

- Pd flower-like nanostructured networks was prepared via a novel CO-assistant method.
- The size and morphology of the materials are temperature depended.
- The novel materials indicated enhanced activity for formic acid electrooxidation.

GRAPHICAL ABSTRACT

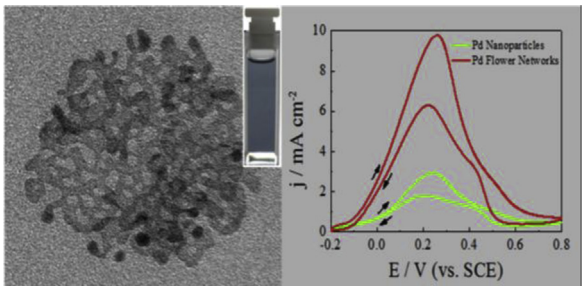

ARTICLE INFO

Article history:
Received 25 February 2014
Received in revised form
20 May 2014
Accepted 21 May 2014
Available online 2 June 2014

Keywords:
Flower-like networks
Palladium
Formic acid oxidation
Electrocatalysis

ABSTRACT

Novel Pd flower-like nanostructured networks are synthesized via a simple CO-assisted reduction. The morphology and size of the Pd nanostructures are found to strongly depend on the temperature and solvent during the synthesis process. Such Pd flower-like nanostructured networks exhibit a much enhanced activity of about 3 times of that on conventional Pd nanoparticles towards the electrocatalytic oxidation of formic acid. The specific activity of formic acid oxidation on Pd nanostructures is also greatly improved, indicating that the formation of flower-like nanostructured networks is beneficial for the electrooxidation of formic acid. Thus, it could be served as highly active catalyst for formic acid electrooxidation although the stability needs to be greatly improved.

1. Introduction

Recently direct formic acid fuel cells (DFAFCs) have attracted increasing attention due to their high energy density and convenient storage and transport of liquid formic acid, etc [1–5]. To date, as the prevailing catalysts for the electrocatalytic oxidation of formic acid [6,7], Pt and Pd based catalysts have been the research focuses. And, Pd is now deemed as the best choice due to its superior initial electrocatalytic activity and a relatively low cost compared to Pt. However, the activity and durability of Pd-based catalysts towards formic acid oxidation is seriously restricted by $(CO)_{ad}$-like poisoning species and possible dissolution of Pd species in acidic solutions [8,9]. The synthesis of high performance Pd-based catalysts thus turns out to be a hot topic. Preparation of Pd with special morphology has been considered as an effective method to improve the performance for formic acid oxidation [10–14].

* Corresponding authors. Tel./fax: +86 21 20321112.
E-mail addresses: yuant@sari.ac.cn (T. Yuan), yangh@sari.ac.cn, huiyang65@hotmail.com (H. Yang).

http://dx.doi.org/10.1016/j.jpowsour.2014.05.113
0378-7753/

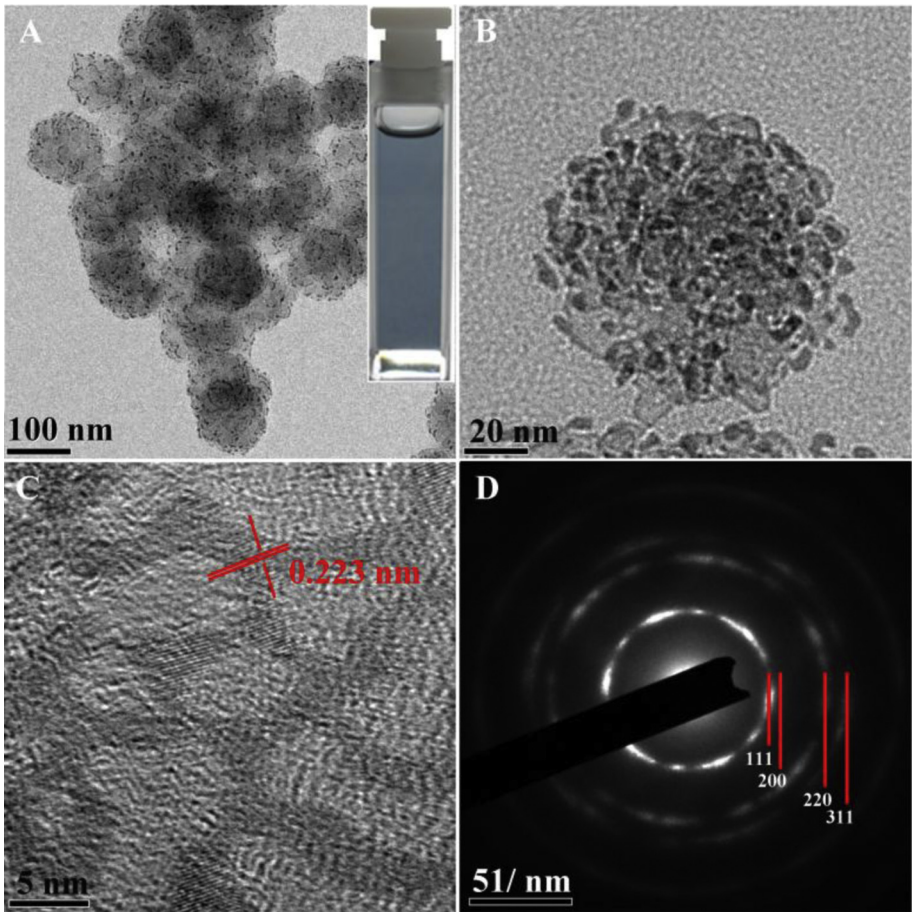

Fig. 1. (A–B) TEM images of Pd FN00 synthesized at 0 °C. Inset in A: photograph of the resultant colloid. (C) HRTEM image of the network. (D) SAED pattern of the network.

Pd has been currently modulated to various nanostructures with well-defined morphologies such as cubes, tetrapods, bipyramidals, freestanding nanosheets, and nanowire networks [10–14]. Among these, highly dispersed and uniform Pd nanowire networks have demonstrated improved electrocatalytic activity for formic acid oxidation depending on the aspect ratio of the nanowires compared to the conventional Pd nanoparticles (NPs) [12,15]. Recent work by Tang et al. has revealed that the use of Pd–Co 3-dimension network catalyst leads to a greatly enhanced catalytic activity and durability towards the oxidation of formic acid owing to their excellent electrochemical self-stability [16]. Herein, we describe a simple CO-assisted synthesis of novel Pd flower-like nanostructured networks (Pd FNs). Such Pd FNs materials can provide much enhanced catalytic activity for the oxidation of formic acid relative to the conventional Pd NPs.

The Pd FNs catalysts were prepared using polyvinyl pyrrolidone (PVP) as a stabilizer and CO as reducing and capping agents in methanol solution at different temperatures. For a comparison, Pd NPs were also prepared with a similar procedure but in an aqueous solution.

2. Experimental section

2.1. Preparation of catalysts

Palladium chloride ($PdCl_2$, AR), sodium chloride (NaCl, AR), PVP (K30, MW = 40,000), methanol (AR), formic acid (AR), and perchloric acid (AR) were purchased from SinoPharm Chemical Reagent Co. Ltd (SCRC). High-purity CO and N_2 were obtained from Air Products and Chemicals, Inc. All the chemicals were used as received.

210 mg PVP and 100 mL of 3.876 mM Na_2PdCl_4/methanol solution was added into a flask. Then, high-purity N_2 was purged into the flask to remove the air in the mixture by stirring violently at a certain temperature (FN00 at 0 °C, FN25 at 25 °C, and FN50 at 50 °C,

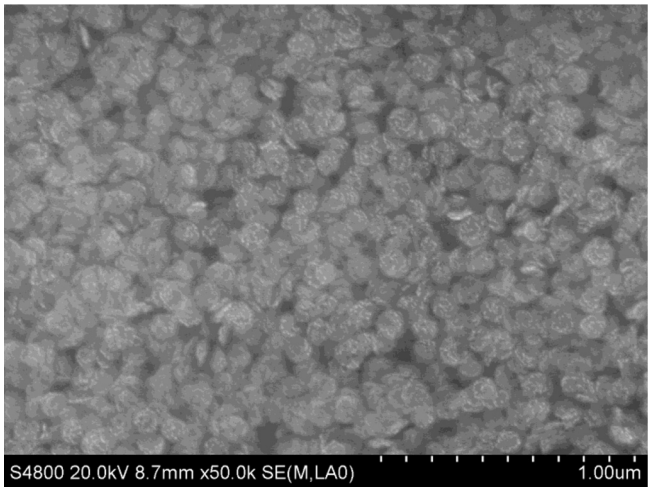

Fig. 2. SEM image of the Pd FN00.

respectively) for 1 h. Thereafter, CO was introduced into the flask at a flow rate of 200 mL min^{-1} under a gentle stirring. After CO purging for 10 min, a CO filled balloon was used to provide CO atmosphere for the reaction system for another 5 h. Finally, the Pd FNs catalysts were collected by filtration, washed with acetone and water for more than 5 times and dried under vacuum for 12 h at 40 °C. Pd sphere nanoparticles were prepared at 25 °C using a similar procedure but in aqueous solution.

2.2. Physical characterization

Transmission electron microscopy (TEM) and high resolution TEM (HR-TEM) characterizations were carried out on a JEOL JEM-2100F TEM. The samples were prepared by ultrasonically suspending the catalyst powder in water. A drop of suspension was then placed onto a holey copper grid and dried in air. Scanning electron microscopy (SEM) characterization was conducted on a HITACHI S-4700 SEM.

2.3. Electrochemical evaluation of catalysts

Electrochemical experiments were carried out using CHI 730B Potentiostat and with a conventional three-electrode cell. The Pd catalyst (10 mg), Nafion solution (0.5 mL of 5 wt. %), and ultrapure water (2.5 mL) were mixed ultrasonically to form the catalyst ink. Subsequently, 3 μL of above ink was transferred onto the surface of a glassy carbon (GC, 3 mm in diameter) electrode using a microsyringe. The electrolyte used was 0.1 M $HClO_4$ or 0.1 M $HClO_4$ + 0.1 M HCOOH. High-purity nitrogen was used for the deaeration of the solutions. In all cases, electrochemical measurements were conducted at a temperature of 25 ± 1 °C.

3. Results and discussion

TEM images in Fig. 1A clearly reveal the formation of Pd flower-like nanostructures, synthesized at 0 °C (Pd FN00), and the inset shows that the resultant colloid solution is in dark blue (in the web version). The mean diameter of the flowers based on an average of more than 100 individuals is 96.8 nm. Notably, a huge number of Pd NPs, like stamens or pollens, are well-distributed on the surface of the flowers, as can be seen in Fig. 1A and B. The mean diameter of Pd NPs on the surface is about 3.80 nm. Further HRTEM image focused on an area without any NPs (Fig. 1C) clearly confirms the formation of Pd nanostructured network. The observed lattice fringe distance of 0.223 nm can be assigned to the Pd (111) facet [17–19]. Interestingly, the observed lattice fringes are continuous along the network, suggesting a sequential growth of the Pd nanocrystals during the synthesis. The crystal structure of the Pd FN00 was further analyzed using selected-area electron diffraction (SAED), as shown in Fig. 1D. The SAED pattern contains a set of diffraction rings denoted as (111), (200), (220) and (311), which can be assigned to the face-centered-cubic (fcc) structure of the Pd [20,21]. SEM image in Fig. 2 presents more visual flower-like morphologies of the Pd FN00.

Further investigations find that the formation of Pd FNs is temperature sensitive during the synthesis. When the reaction temperature was raised to 25 and 50 °C, the resultant mixture of Pd FN25 was still in dark blue; but the Pd FN50 turns out to be black.

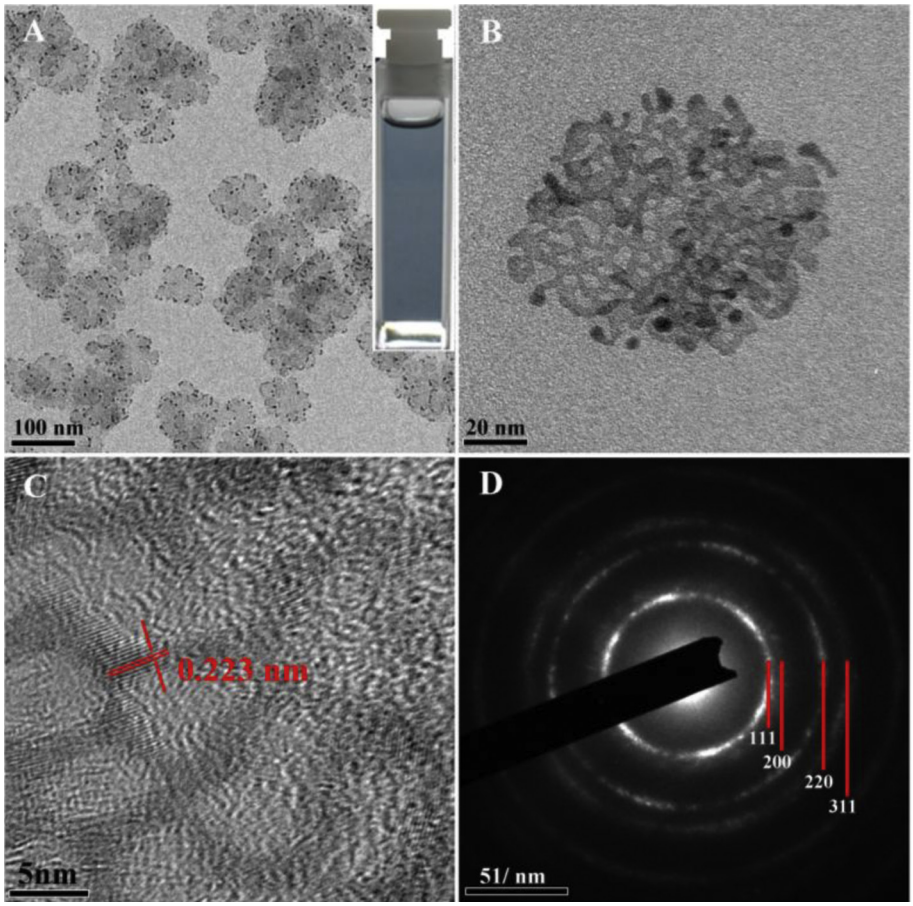

Fig. 3. (A–B) TEM images of the Pd FN25, synthesized at 25 °C. Inset in A: photograph of the resultant colloid. (C) HRTEM image of the network. (D) SAED pattern of the network.

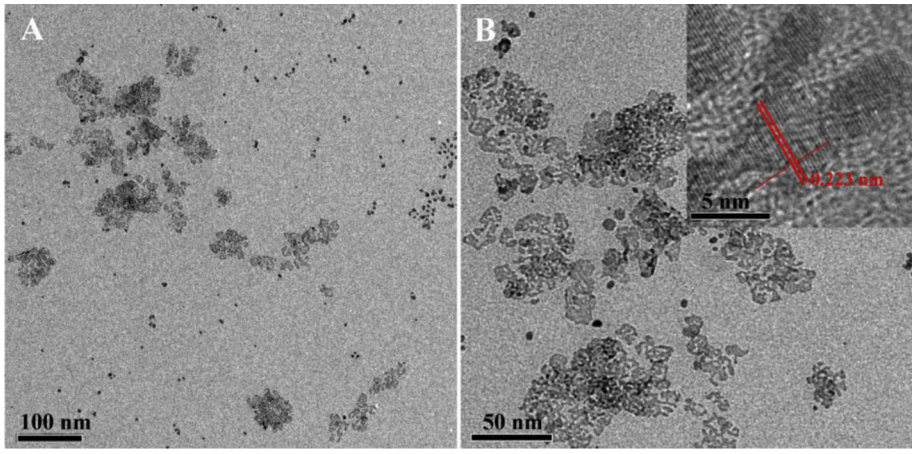

Fig. 4. TEM images of the Pd FN50 (A–B). Inset in B: HRTEM image.

The difference in solution color might be an indicator of the reaction rate. TEM images in Fig. 3A and B shows obvious flower-like structure of the Pd FN25 with a decreased mean diameter of 81.6 nm. Interestingly, Pd FN25 shows much less Pd NPs distributed on the surface of the flower-like nanostructures in comparison to the Pd FN00. HRTEM image in Fig. 3C again demonstrates the formation of Pd network with the Pd (111) lattice fringe clearly visible. The SAED pattern in Fig. 3D also confirms the Pd fcc structure of the Pd FN25. When the synthesis temperature increases to 50 °C, however, irregular networks with some isolated NPs can be obtained, as can be seen in Fig. 4.

From above results, it is clear that the morphology and size of the Pd FNs strongly depend on the temperature and solvent during the synthesis process. Generally, a much faster "nucleation" process would happen at high temperature once CO was introduced as reducing agent, and more Pd seeds would be formed during "evolution of nuclei into seeds", implying that less residual precursor exists in the solution. Hence, the subsequent growth of seeds into nanocrystals, due to an insufficient amount of Pd precursor in the solution, would lead to the formation of small-size nanostructures. On the contrary, the synthesis of Pd nanostructures at lower temperature would result in a slower reduction of the precursor. In this case, Pd FNs with big size would be formed [22,23]. The Pd NPs on the surface of Pd FNs might be due to the presence of small amount of water in methanol solution.

Also, carbon monoxide was employed as both reducing agent and capping agent for the synthesis of Pd FNs. As reported, CO would preferentially adsorb on the Pd (111) surface, thus facilitating the growth of nanocrystals having (111) as the main exposure surface [24]. Previous synthesis of freestanding Pd nanosheets has indicated that the introduction of CO plays a crucial role for the anisotropic growth in a 2-dimensional plane [10]. In the meantime, the control of reduction kinetics by CO could facilitate one dimensional growth of metals [25]. Accordingly, CO seems to play the similar roles in our synthesis procedure. Thus, the combination of both anisotropic growth and one dimensional growth of Pd nanostructures could be responsible for the formation of Pd FNs.

Furthermore, TEM image of as-prepared Pd NPs synthesized in pure water, as shown in Fig. 5, indicates that the mean diameter of Pd NPs is ca. 3.87 nm with a very narrow particle size distribution.

The electrochemical performance of the Pd FNs and Pd NPs catalysts were compared on GC electrodes with the same Pd

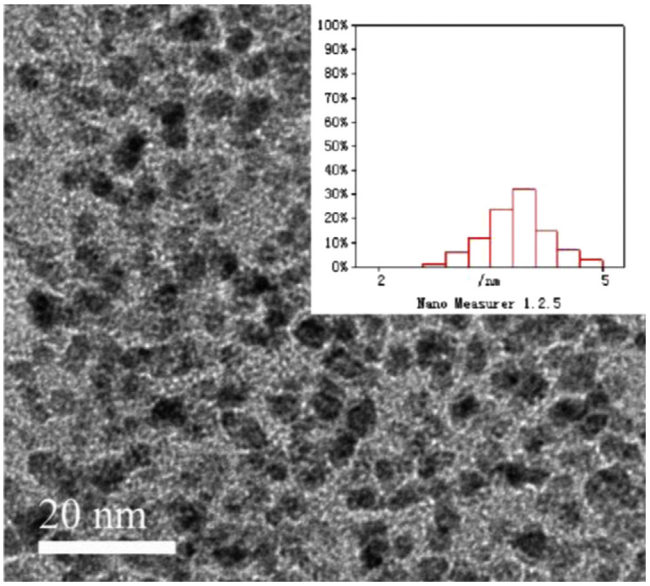

Fig. 5. TEM image and size distribution diagram (inset) of the Pd NPs synthesized in an aqueous solution.

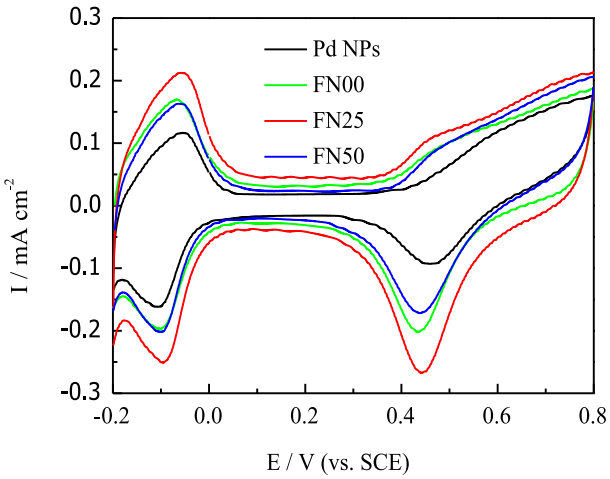

Fig. 6. CVs of the Pd FNs and Pd NPs at a scan rate of 50 mV s^{-1} in 0.1 M $HClO_4$ solution.

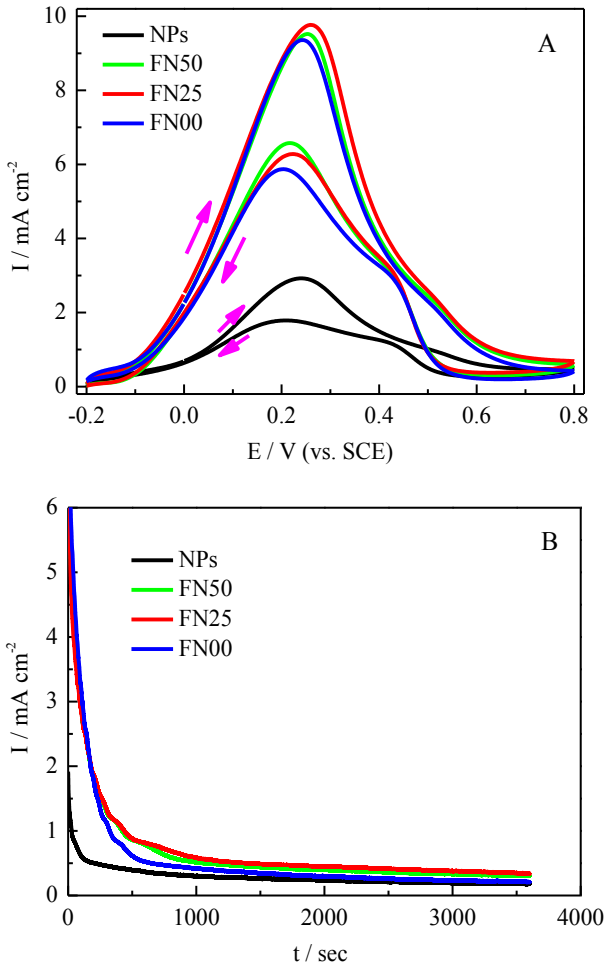

Fig. 7. (A) CVs at a scan rate of 50 mV s^{-1} and (B) *i*–*t* curves at 0.16 V (vs. SCE) on the Pd FNs and Pd NPs catalysts in 0.1 M $HClO_4$ + 0.1 M HCOOH.

loading of 141.5 μg cm^{-2}. The potential of Pd based electrodes was firstly held at −0.292 V (vs. SCE) in 0.1 M $HClO_4$ for 5 min to remove the residual PVP [26]. Fig. 6 shows typical cyclic voltammograms (CVs) of different Pd samples. By calculating the hydrogen desorption region area, the electrochemical surface areas (ECSAs) are estimated as 8.89, 9.03, 8.74 and 6.47 m^2 g^{-1} for the Pd FN00, Pd FN25, Pd FN50 and Pd NPs, respectively; indicating that the Pd FNs exhibit higher ECSAs than Pd NPs. It is believed that the use of the highly interconnected Pd FN networks might be beneficial for the formation of porous electrode, which could account for the enhanced ECSA with Pd FNs. Fig. 7A is a comparison of the CVs on the Pd FNs and Pd NPs catalysts in 0.1 M HCOOH + 0.1 M $HClO_4$ at a scan rate of 50 mV s^{-1}. Current densities of formic acid oxidation on different Pd FNs catalysts are very close to each other, but are much higher than that on the Pd NPs. And the maximum peak current density on the Pd FN25 is about 3.0 times of that on the Pd NPs. Further comparison at a potential of 0.16 V/SCE also reveals that the current density of formic acid oxidation on the Pd FN25 is ca. 3.2 times of that on the Pd NPs. Based on ECSAs, the peak specific activities on the Pd FNs are about 2–2.4 times of that on the Pd NPs, again assessing that the Pd FNs exhibit much enhanced catalytic activity for formic acid oxidation.

Fig. 7B illustrates *i*–*t* curves of the Pd FNs and Pd NPs catalysts at a given potential of 0.16 V/SCE in 0.1 M HCOOH + 0.1 M $HClO_4$. A much higher initial current density of formic acid oxidation on Pd FNs is observed relative to that on the Pd NPs. And the current densities on the Pd FNs catalysts are still much higher than that on the Pd NPs even after 1 h polarization. And at this point, the current density of formic acid oxidation on the Pd FN25 is still about 2 times of that on the Pd NPs. Nevertheless, the activity decay on the Pd FNs is faster than that on the Pd NPs, which could be due to the fact that much enhanced catalytic activity would accelerate the production and accumulation of carbon-containing intermediates, thus resulting in a quick poisoning of the catalyst [7,9,27,28]. Thus, to improve the durability of Pd FNs, alloying with other metals such as Co, Pb, Au would be an efficient way to avoid possible poisoning. Alternatively, anchoring Pd FNs on carbon support would be another way to prevent the Pd NFs from possible dissolution and/or from Pd aggregation in acidic environment [16,29–32].

4. Conclusions

In summary, we have reported the successful synthesis of novel Pd flower-like nanostructure network catalysts for formic acid oxidation. The Pd FNs catalysts exhibit greatly enhanced mass activity and specific activity for the oxidation of formic acid relative to the Pd NPs. Since Pd-based network catalysts currently are found very efficient for catalytic process, this study is of great significance for the research of similar materials.

Acknowledgments

This work was financially supported by the National Basic Research Program of China (973 Program) (2012CB932800), the National Natural Science Foundation of China (21073219), Shanghai Science and Technology Committee (11DZ1200400), the Knowledge Innovation Engineering of the CAS (12406, 124091231), the Scientific and Technological Innovation Fund for Graduate Students of the CAS, and Drexel-SARI Global Funding Scheme.

References

[1] Y.L. Qin, J. Wang, F.Z. Meng, L.M. Wang, X.B. Zhang, Chem. Commun. (Camb.) 49 (2013) 10028–10030.
[2] Y.-Y. Feng, G.-R. Zhang, B.-Q. Xu, RSC Adv. 3 (2013) 1748–1752.
[3] J.-Y. Wang, Y.-Y. Kang, H. Yang, W.-B. Cai, J. Phys. Chem. C 113 (2009) 8366–8372.
[4] K. Tedsree, T. Li, S. Jones, C.W.A. Chan, K.M.K. Yu, P.A.J. Bagot, E.A. Marquis, G.D.W. Smith, S.C.E. Tsang, Nat. Nanotechnol. 6 (2011) 302–307.
[5] Z. Bai, L. Yang, J. Zhang, L. Li, J. Lv, C. Hu, J. Zhou, Catal. Commun. 11 (2010) 919–922.
[6] D.-J. Chen, Z.-Y. Zhou, Q. Wang, D.-M. Xiang, N. Tian, S.-G. Sun, Chem. Commun. 46 (2010) 4252–4254.
[7] M. Ren, Y. Kang, W. He, Z. Zou, X. Xue, D.L. Akins, H. Yang, S. Feng, Appl. Catal. B 104 (2011) 49–53.
[8] S. Zhang, Y. Shao, G. Yin, Y. Lin, Angew. Chem. Int. Ed. 49 (2010) 2211–2214.
[9] J.-Y. Wang, H.-X. Zhang, K. Jiang, W.-B. Cai, J. Am. Chem. Soc. 133 (2011) 14876–14879.
[10] X. Huang, S. Tang, X. Mu, Y. Dai, G. Chen, Z. Zhou, F. Ruan, Z. Yang, N. Zheng, Nat. Nanotechnol. 6 (2011) 28–32.
[11] Y. Dai, X. Mu, Y. Tan, K. Lin, Z. Yang, N. Zheng, G. Fu, J. Am. Chem. Soc. 134 (2012) 7073–7080.
[12] S. Wang, X. Wang, S.P. Jiang, Nanotechnology 19 (2008) 455602.
[13] X. Huang, S. Tang, H. Zhang, Z. Zhou, N. Zheng, J. Am. Chem. Soc. 131 (2009) 13916–13917.
[14] X. Xia, S.I. Choi, J.A. Herron, N. Lu, J. Scaranto, H.C. Peng, J. Wang, M. Mavrikakis, M.J. Kim, Y. Xia, J. Am. Chem. Soc. 135 (2013) 15706–15709.
[15] J. Wang, Y. Chen, H. Liu, R. Li, X. Sun, Electrochem. Commun. 12 (2010) 219–222.
[16] L. Zhang, L. Wan, Y. Ma, Y. Chen, Y. Zhou, Y. Tang, T. Lu, Appl. Catal. B 138–139 (2013) 229–235.
[17] M. Ren, J. Chen, Y. Li, H. Zhang, Z. Zou, X. Li, H. Yang, J. Power Sources 246 (2014) 32–38.
[18] C. Xu, A. Liu, H. Qiu, Y. Liu, Electrochem. Commun. 13 (2011) 766–769.
[19] R. Wang, H. Wang, X. Wang, S. Liao, V. Linkov, S. Ji, Int. J. Hydrogen Energy 38 (2013) 13125–13131.
[20] L. Zhang, L. Liu, X. Cheng, Y. Zhang, Q. Fan, Mater. Chem. Phys. 127 (2011) 62–69.
[21] D. Zhu, L. Zhang, M. Song, X. Wang, Y. Chen, Chem. Commun. 49 (2013) 9573–9575.

[22] Y. Xia, Y. Xiong, B. Lim, S.E. Skrabalak, Angew. Chem. Int. Ed. 49 (2009) 60–103.
[23] Y. Xiong, Y. Xia, Adv. Mater. 19 (2007) 3385–3391.
[24] M. Chen, B. Wu, J. Yang, N. Zheng, Adv. Mater. 24 (2012) 862–879.
[25] Y. Kang, X. Ye, C.B. Murray, Angew. Chem. Int. Ed. 49 (2010) 6156–6159.
[26] M. Shao, J. Odell, M. Humbert, T. Yu, Y. Xia, J. Phys. Chem. C 117 (2013) 4172–4180.
[27] A. Mikołajczuk, A. Borodzinski, P. Kedzierzawski, L. Stobinski, B. Mierzwa, R. Dziura, Appl. Surf. Sci. 257 (2011) 8211–8214.
[28] W.S. Jung, J. Han, S.P. Yoon, S.W. Nam, T.-H. Lim, S.-A. Hong, J. Power Sources 196 (2011) 4573–4578.
[29] H. Hosseini, M. Mahyari, A. Bagheri, A. Shaabani, J. Power Sources 247 (2014) 70–77.
[30] J. Chai, F. Li, Y. Hu, Q. Zhang, D. Han, L. Niu, J. Mater. Chem. 21 (2011) 17922–17929.
[31] R.D. Morgan, A. Salehi-khojin, R.I. Masel, J. Phys. Chem. C 115 (2011) 19413–19418.
[32] X. Yu, P.G. Pickup, J. Power Sources 192 (2009) 279–284.